

AD-A276 780



2

OFFICE OF NAVAL RESEARCH

Contract No. N00014-91-J-1409

Technical Report No. 146

Nanoscale Structural Changes Upon Electrooxidation of Au(111) as Probed by Potentiodynamic Scanning Tunneling Microscopy

by

Xiaoping Gao and Michael J. Weaver

DTIC ELECTE MAR 10 1994 S E D

Prepared for Publication

in

Journal of Electroanalytical Chemistry

Department of Chemistry

Purdue University

West Lafayette, Indiana 47907-1393

February 1994

Accession For	
NTIS CRA&I	<input checked="" type="checkbox"/>
DTIC TAB	<input type="checkbox"/>
Unannounced	<input type="checkbox"/>
Justification	
By	
Distribution /	
Availability Codes	
Dist	Avail and/or Special
A-1	

94-07829

Reproduction in whole, or in part, is permitted for any purpose of the United States Government.

\* This document has been approved for public release and sale; its distribution is unlimited.

94 3 9 076

Understanding the surface structural changes associated with, and resulting from, the electrochemical formation and removal of oxide films is of broadbased practical as well as fundamental importance. Studies of noble metals, such as gold and platinum, are of particular interest in this context. The recent emergence of scanning tunneling microscopy (STM) as an in-situ tool of electrochemical surface structure is providing substantial new opportunities for understanding metal surface oxidation, alongside a myriad of other issues, at the atomic level. At the current state of development of STM, monocrystalline gold electrodes provide efficacious choices of systems, partly in view of their chemical inertness as well as ease of preparation of well-ordered surfaces by means of flame-annealing procedures[1]. Not surprisingly, then, several in-situ STM studies have focussed on the surface morphological changes attending oxidation and rereduction of single-crystal gold electrodes, chiefly Au(111)[2-7]. A related study using atomic force microscopy (AFM) has also appeared[8].

These reports chiefly involve STM imaging at a series of fixed potentials, either before and after voltammetric formation and removal of oxide layers[2,5], or additionally at suitably high electrode potentials so that surface oxide is present[3,4,6,7]. Evident are several characteristic oxide-induced changes in surface morphology, including the formation of monolayer "pits" and related metal corrosion, disordering, and roughening. Of the unanswered questions, a central issue concerns the links between surface structural changes and the much-discussed voltammetric features for the initial oxidation of ordered gold electrodes[9,10]. We have employed increasingly a tactic for gold and other electrodes, dubbed "potentiodynamic" STM (PDSTM), which entails acquiring individual images (or sequences of images) during electrode-potential excursions, arranged so that the potential-induced structural changes appear as alterations in the imaging characteristics along the y direction (time/space coordinate)[11-

14]. The virtues of PDSTM include the ability to decipher precise lattice geometries and binding sites for ordered adlayers[11,12], and to aid the detection of more subtle potential-induced changes, such as surface phase transitions[13]. The application of PDSTM during potential-sweep excursions, in particular, offers direct connections to be made with current-potential features in simultaneously acquired voltammetric data[13].

We describe here some observations using this tactic for the electrooxidation and rereduction of ordered Au(111) in aqueous 0.1 M HClO<sub>4</sub> and H<sub>2</sub>SO<sub>4</sub> electrolytes. The findings provide some fresh insight into the surface atomic-scale morphological changes associated with the well-known voltammetric features.

The experimental STM procedures largely are described elsewhere[15,16]. The microscope is a Nanoscope II (Digital Instruments) with a bipotentiostat for in-situ electrochemical STM. The STM tips were iridium wires, sharpened by mechanical polishing and insulated with a thermosetting polyethylene plastic or Apiezon wax[13]. The Au(111) surface (hemisphere, 5 mm diameter) was prepared at CNRS, Meudon, France by Dr. A. Hamelin. It was pretreated by flame annealing, and cooled partly in air and in ultrapure water immediately before transfer to the STM cell[13]. The counter electrode was a gold wire, and the quasi-reference electrode was an electrooxidized gold wire. All electrode potentials quoted here, however, are converted to the normal hydrogen electrode (NHE) scale.

The basic tactic followed here was to record appropriate sequences of STM images, the acquisition of each consuming ca 20 s, during voltammetric potential excursions, typically from potentials well within the double-layer region on gold (around 0.8 V vs NHE) to suitably high potentials (usually from 1.6-1.8 V) and return, so to engender at least initial surface oxidation followed by reduction. (The tip potential was varied only up to ca 1.1 V vs NHE, so to avoid Ir

electrooxidation; the acquisition of images for markedly higher substrate potentials therefore involved commensurate alterations in the bias potential.) The potential sweep rate varied from 5–50  $\text{mV s}^{-1}$ . The solid trace in Fig. 1 shows a typical voltammogram recorded in the STM cell at 50  $\text{mV s}^{-1}$  for Au(111) in 0.1 M  $\text{HClO}_4$ . The appearance of the voltammetric features diagnostic of surface oxidation compares favorably with published data obtained under ultraclean electrochemical conditions[1,10]. Thus, the two characteristic anodic peaks for Au(111) at about 1.3 and 1.5 V (labelled OA3 and OA4 in refs. 9 and 10) are clearly apparent, with a low-potential "tail" on the former (resolved earlier as OA1 and OA2[9,10]), together with the sharp oxide reduction wave on the reverse potential sweep. However, such voltammograms were obtained prior to introducing the STM tip and piezo head assembly. The presence of the tip in the solution over the lengthy (ca 1–2 hour) periods often necessary to acquire the STM data yields some voltammetric degradation caused by surface contamination by the tip insulating material. The dashed segment in Fig. 1 is a typical case: the OA3 feature is muted somewhat even though OA4 remains largely unaffected. Such effects should therefore be borne in mind when considering the STM data below.

Figures 2A–E show a sequence of five STM images for a large (ca 140 nm) square area obtained at a constant tunneling current (1 nA) on Au(111) in 0.1 M  $\text{HClO}_4$  during a potential excursion from 0.85 V to 1.8 V vs NHE and return at 20  $\text{mV s}^{-1}$ . The first image (A) was obtained by rastering the tip downwards while sweeping the potential from 0.8 to 1.2 V. A pair of largely uniform terraces is discerned, separated by a step running near-vertically down the middle. Close-up images yielded clear atomic-resolution ( $1 \times 1$ ) arrays[13,16]. The second (upward rastered) image (B), recorded immediately thereafter, corresponds to a potential region (1.2 to 1.6 V) within which the anodic oxide peaks OA1–3 and 4 are

located. During the excursion through the former feature (corresponding to the bottom third of the image), the terrace edge is seen to become diffuse. (This feature was discerned even more clearly in a number of the images taken in the OA3 potential region.) More prominently, the surface becomes "rougher" in a potential region (ca 1.45–1.55 V, commencing just into the upper half of the image), which encompasses the major anodic oxidation peak OA4 (Fig. 1). This roughness is typically atomic-scale (0.2–0.3 nm) in height (z-direction) but large enough in the surface plane (2–4 nm) to suggest the presence of gold oxide "clustering". This roughness is seen to be attenuated at potentials beyond 1.55 V in the voltammetric cycle, as discerned from the top 20% of B, and throughout the ensuing downward-rastered image (traversing 1.6 to 1.8 and return to 1.6 V), not shown in Fig. 2. The terrace edge is also typically "shifted" significantly, by ca 2–5 nm, towards the lower terrace upon traversing OA4.

The voltammetric feature OA1–3 and OA4 have been interpreted in terms of the processes[9,10]:



Place exchange of the oxygen and Au atoms has been deduced to occur during the latter stages of OA1–3 as well as throughout OA4 in the basis of the electrochemical irreversibility of these processes[9]. The observed occurrence of nanoscale surface roughening during OA4 is consistent with this well-known notion. The apparent absence of such roughening during OA3 thereby might be thought to be at odds with the assertion of place exchange. We suspect, however, that this disparity is perhaps illusory. Thus the changes in both the position and "sharpness" of the gold terrace edges seen during OA3 suggest that the

surface gold lattice dimensions are being altered by reaction (1a). Such a structural change is indicative of a significant alteration of the gold lattice structure, portending at least a surface relaxation associated with partly ionic  $\text{Au}^{4+} - \text{OH}^{4-}$  bond formation if not complete place exchange. Such a surface rearrangement should engender electrochemical irreversibility, as is observed. It is appropriate, nonetheless, to suspect possible complications from surface contamination by the tip coating (vide supra).

These findings are essentially consistent with those of Itaya and coworkers[3], who observed some Au(111) surface roughening upon holding at about 1.45 V, which was attenuated after increasing the potential to 1.65 V. [Note, however, that the constant-potential imaging procedure used in ref. 3, necessarily observes the structural consequences following potential perturbations, while the present PDSTM tactic monitors the potential-dependent evolution of the structural changes (cf ref. 4)].

Images C-E in Fig. 2 complete the string of STM scans obtained during the return voltammetric sweep, specifically from ca 1.6 to 1.2 V, 1.2 to 0.8 V, and 0.8 to 0.4 V vs NHE, while rastering the tip upwards, downwards, and again upwards, respectively. Only minor variations in the image characteristics are seen in the interval 1.6 to 1.2 V(C), chiefly at about 1.3 V (i.e. within 20% of the top of image C). Not surprisingly, more drastic changes are seen upon initiating the oxide rereduction, as discerned by the onset of the cathodic wave at 1.1 V (Fig. 1), corresponding to a point ca 20% from the top of image D. At this point, a marked roughening of the surface is clearly discerned, dense arrays of cavities being formed. Close to the cessation of the major voltammetric reduction peak, corresponding to halfway down the imaged area in C (about 1.05 V), arrays of gold protrusions ("islands") begin to be more evident along with the cavities ("pits"); the former increase in size, from 5 nm, as the tip

traverses towards the bottom of image D. Oxide reduction is also seen to shift the terrace edge back towards the left-hand side of the imaged area.

Further information concerning the origin of these oxide-induced nanoscale features is discerned from the following image (E). The tip is again rastered in E in the opposite direction (upward) from its immediate predecessor (D), but now following completion of the oxidation-reduction cycle. Two features of E are seen clearly to differ from D. First, the islands in E are larger yet less dense than in D. This is true especially towards the center of the images, corresponding to a larger time lag between D and E. This change, which is accompanied by a diminution in the average pit size, therefore indicates that these gold clusters undergo substantial aggregation within ca 20 s or so. The second point of interest concerns the appearance of larger (ca 10 nm) pits in the upper portion of E corresponding to the surface region where the tip was rastered in D during the oxide reduction wave. The appearance of these pits, together with the relative dearth of nearby islands, indicates that they are created largely by the scanning STM tip while voltammetric oxide reduction is proceeding.

The clear observation of such a potential-dependent invasive effect by PDSTM raises the possibility that other surface morphological changes seen in Fig 2A-E may also arise from tip-scan effects. Figure 2F is an image, shown with this point in mind, obtained at 0.6 V six minutes after Fig. 2E but for a larger scan area so that the top one-third of F is a surface region not scanned by the tip during the previous oxidation-reduction cycle (as interrogated by images A-E). Significantly, the surface morphology of this upper terrace region is essentially the same as the lower imaged area in F, although only the latter experienced tip scanning during or following surface oxidation. Note that the middle-center portion of F shows the larger pits, also seen in E, formed by tip scanning during oxide reduction.

Both Trevor et al[2] and Honbo et al[3] report the presence of monoatomic pits, similar to those observed here, following oxide reduction on Au(111); the former authors note that substantial pit formation (in the absence of tip scanning during the voltammetric cycle) requires potential excursions to at least 1.8 V vs NHE. Figure 3A-D shows the latter portion of a PDSTM sequence obtained during a  $10 \text{ mV s}^{-1}$  potential excursion up to only 1.7 V, but at a higher tunneling current, 10 nA, than for Fig 2. The first image, A, is a downward rastered scan taken as the potential was swept from ca 1.45 to 1.2 V. Some noticeable "roughening" is seen to appear by about halfway down the image (i.e. by ca 1.3 V), i.e. just before the onset of the oxide reduction wave (Fig 1). (This observation suggests the occurrence of a surface structural change as a precursor to the oxide reduction process, although the occurrence of an invasive tip effect cannot be ruled out.) The following upward-rastered image C, obtained during and after the latter portion of oxide reduction, again shows a marked appearance of pits following the subsidence of roughness. These pits, however, are formed at least partly by the scanning tip, as demonstrated by images C and D, the latter being obtained at 0.6 V one min. afterward. The former image shows the complete area scanned by the tip during the oxidation-reduction cycle, whereas the latter displays a region partly to the left of this area. The near-absence of pits in the previously unscanned region in D demonstrates that the pits seen in C were created largely by the tip rastering across the oxidized surface. These include pits formed by the tip scanning prior to, as well as during, oxide reduction. (Note, however, that the latter pits are particularly large.) This difference with the behavior discerned from Fig 2F results from the larger tunneling current (i.e. smaller substrate-tip distances) employed in Fig 3. Thus PDSTM data acquired at smaller tunneling currents ( $< 2$  to  $5 \text{ nA}$ ) show only sparse pit formation for potential excursions to 1.7 V or below. Similar

PDSTM results were obtained under these conditions when 0.1 M  $\text{H}_2\text{SO}_4$  was substituted for 0.1 M  $\text{HClO}_4$ , although the OA3 peak is suppressed in the former electrolyte and an ordered adlayer ("adsorbed bisulfate") structure is discernable above 1.0 V prior to the onset of surface oxidation[17].

These findings shed some light on the likely factors responsible for, as well as the nature of, the surface morphological changes accompanying Au(111) oxidation and rereduction. The metal-oxygen place exchange attending surface oxidation is seen initially to produce arrays of nanoscale clusters along with some apparent expansion of the surface lattice. This suggests that the oxide layer is somewhat disordered. While atomic-resolution images taken at suitably high potentials display some locally (sub-nm) organized arrays, no longer-range ordering of the oxide film structure is discernable. The formation of denser arrays of reduced gold clusters is particularly evident during voltammetric oxide removal. Both oxidized and reduced clusters, but especially the latter, adhere only loosely to the metal surface as evidenced by the tip-induced production of pits and accompanying gold islands upon completion of oxide reduction.

We suggest that the formation of the reduced gold clusters during oxide reduction is a key intermediate step in the overall structural transformations induced by voltammetric cycling. Once formed, the reduced nanoscale clusters may experience three distinct fates. First, they can be reincorporated into the surface metal lattice to become (1 x 1) domains. Second, they may aggregate to form larger monolayer clusters (islands) remaining atop the surface lattice, with accompanying pits being produced. The latter fate would appear to become increasingly likely following potential excursions to above 1.8 V, corresponding to sufficiently extensive oxide formation to engender second-layer place exchange. Nonetheless, over longer time periods (> few minutes), the pits can eventually fuse with nearby islands or become incorporated into terrace edges[2].

The third possible fate involves partial dissolution of the gold clusters as hydrated  $\text{Au}^{3+}$  or  $\text{Au}^+$ . Interestingly, significant dissolution of gold during oxide reduction has been detected by rotating ring-disk voltammetry[18]. It is plausible that the nanoscale reduced gold particles are more susceptible to dissolution than the more energetically stable terrace gold atoms; some formation of  $\text{Au}^{3+}$  might be anticipated at around 1.1 V despite the higher (1.52 V) standard potential of the  $\text{Au}^{3+}/\text{Au}$  couple[19].

#### Acknowledgment

We are grateful to Dr. Antoinette Hamelin for preparing the Au(111) crystal. This work is supported by the Office of Naval Research and the National Science Foundation.

**References**

- 1) A. Hamelin, in "Modern Aspects of Electrochemistry", Vol. 16, B.E. Conway, R.E. White, and J. O'M. Bockris, eds., Plenum, New York, 1986, Chapter 1.
- 2) D.J. Trevor, C.E.D. Chidsey, and D.N. Liacono, Phys. Rev. Lett., 62 (1989), 929.
- 3) H. Honbo, S. Sugawara, and K. Itaya, Anal. Chem., 52 (1990), 2424.
- 4) K.J. Hanson and M.P. Green, Mat. Res. Soc. Symp. Proc., 237 (1992), 323.
- 5) D.J. Trevor and C.E.D. Chidsey, J. Vac. Sci. Tech., B9 (1991), 964.
- 6) C.M. Vitus and A.J. Davenport, Abstract 1925, Electrochemical Society Spring Meeting, Honolulu, HI, May 1993.
- 7) R.J. Nichols, O.M. Magnusson, J. Hotlos, J. Twomey, R.J. Behm, and D.M. Kolb, J. Electroanal. Chem., 290 (1990), 21.
- 8) S. Manne, J. Massie, V.B. Elings, P.K. Hansma, and A.A. Gewirth, J. Vac. Sci. Tech., B9 (1991), 950.
- 9) H. Angerstein-Kozłowska, B.E. Conway, A. Hamelin, and L. Stoicoviciu, J. Electroanal. Chem., 228 (1987), 429.
- 10) H. Angerstein-Kozłowska, B.E. Conway, A. Hamelin, and L. Stoicoviciu, Electrochim. Acta, 31 (1986), 1051.
- 11) X. Gao and M.J. Weaver, J. Am. Chem. Soc., 114 (1992), 8544.
- 12) X. Gao and M.J. Weaver, Ber. Bunsenges. Phys. Chem., 97 (1993), 507.
- 13) X. Gao, G.J. Edens, A. Hamelin, and M.J. Weaver, Surf. Sci., in press.
- 14) X. Gao and M. J. Weaver, J. Phys. Chem., 97 (1993), 8685.
- 15) X. Gao, A. Hamelin, and M.J. Weaver, Phys. Rev. Lett., 67 (1991), 618.
- 16) X. Gao, A. Hamelin, and M.J. Weaver, Phys. Rev. B, 46 (1992), 7096.
- 17) O.M. Magnussen, J. Hageböck, J. Hotlos, and R.J. Behm, Far. Disc., 94 (1992), 329.
- 18) S.H. Cadle and S. Bruckenstein, Anal. Chem., 46 (1974), 16.
- 19) G.M. Schmid, in "Standard Potentials in Aqueous Solution", A.J. Bard, R. Parsons, and J. Jordan, Eds., M. Dekker, New York, 1985, Chapter 11.

### Figure Captions

#### Figure 1

Typical cyclic voltammogram at  $50 \text{ mV s}^{-1}$  recorded in STM cell for Au(111) in  $0.1 \text{ M HClO}_4$ . Dashed trace was obtained after introducing STM tip assembly.

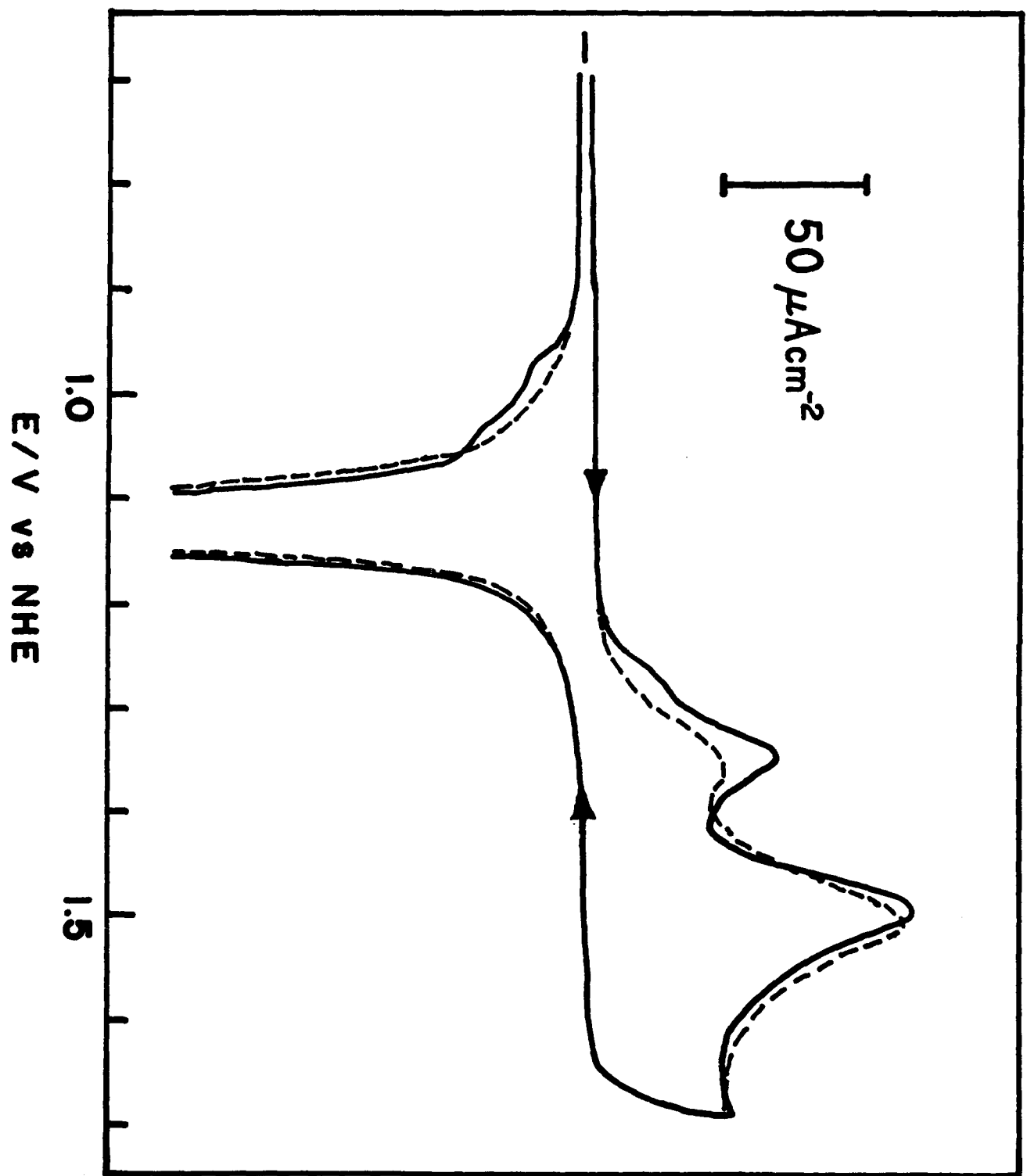
#### Figure 2

Sequence of STM images obtained during  $20 \text{ mV s}^{-1}$  potential excursion from  $0.85 \text{ V}$  to  $1.8 \text{ V}$  vs NHE and return. Tunneling current =  $1 \text{ nA}$ ; tip potential =  $0.65$  to  $1.0 \text{ V}$  vs NHE. Each image acquisition consumed  $20 \text{ s}$ . A) downward tip rastering,  $0.8$  to  $1.2 \text{ V}$ ; B) upward,  $1.2$  to  $1.6 \text{ V}$ ; C) upward,  $1.6$  to  $1.2 \text{ V}$ ; D) downward,  $1.2$  to  $0.8 \text{ V}$ ; E) upward,  $0.8$  to  $0.4 \text{ V}$ ; F) obtained  $6 \text{ min}$  after E at  $0.6 \text{ V}$ , for enlarged scan area (see text).

#### Figure 3

Sequence of STM images obtained during return portion of oxidation-reduction cycle at  $10 \text{ mV s}^{-1}$  from  $0.8$  to  $1.7 \text{ V}$  and return. Tunneling current =  $10 \text{ nA}$ . Each image acquisition consumed  $26 \text{ s}$ . A) downward tip rastering, from ca  $1.45$  to  $1.2 \text{ V}$ ; B) upward, ca  $1.18$  to  $0.92 \text{ V}$ ; C) downward,  $0.92$  to  $0.65 \text{ V}$ ; D) obtained at  $0.6 \text{ V}$ ,  $1 \text{ min}$  after completion of C, with imaged area shifted to left so to include region not scanned by STM tip during voltammetric cycle.

*[Note to printer - if possible, please arrange the photographic figures 2A-F, 3A-D in a similar "block fashion" as displayed in the preprint - this would facilitate intercomparison of members of each sequence by the reader. Also, please ensure that the contrast in the reproduced images is sufficient so that the morphological features are clearly discernable. Thanks!]*



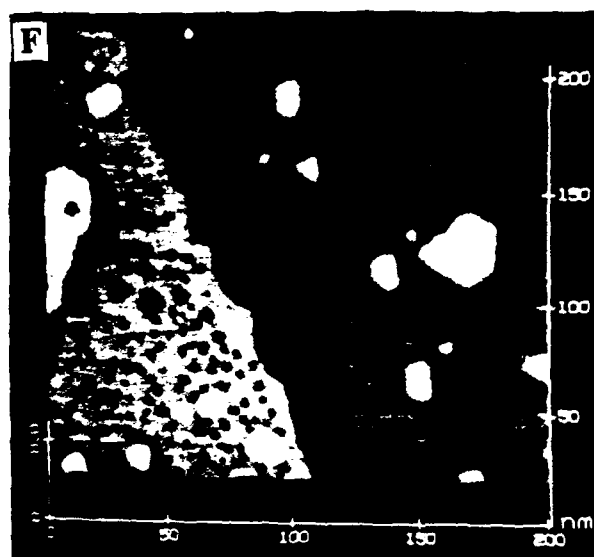
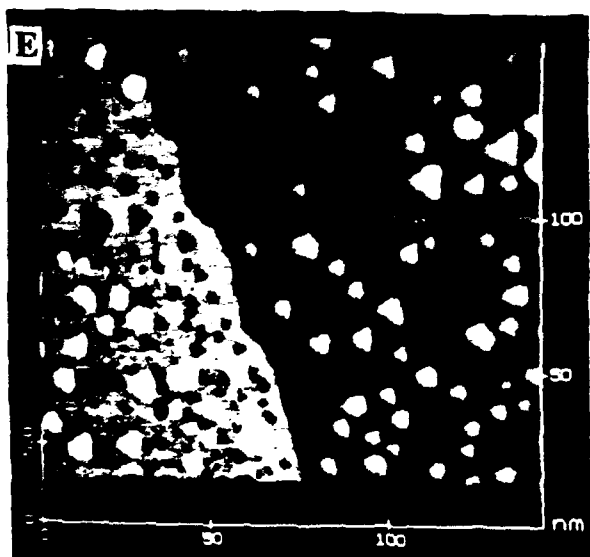
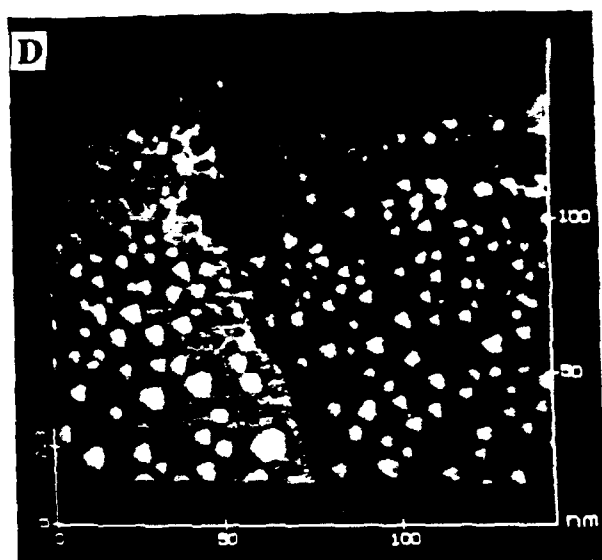
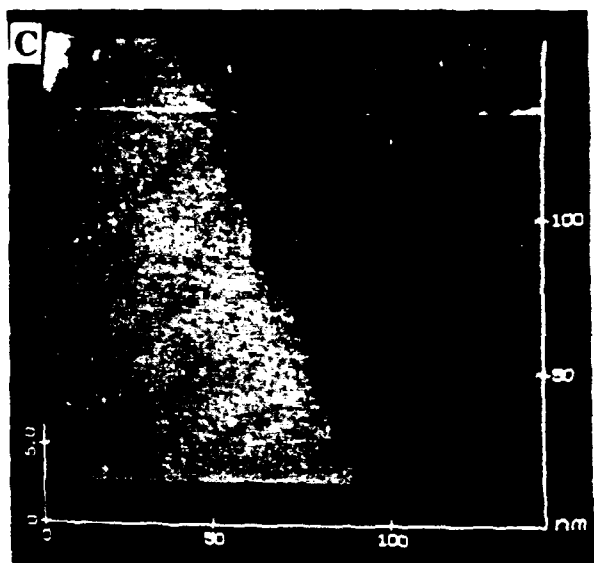
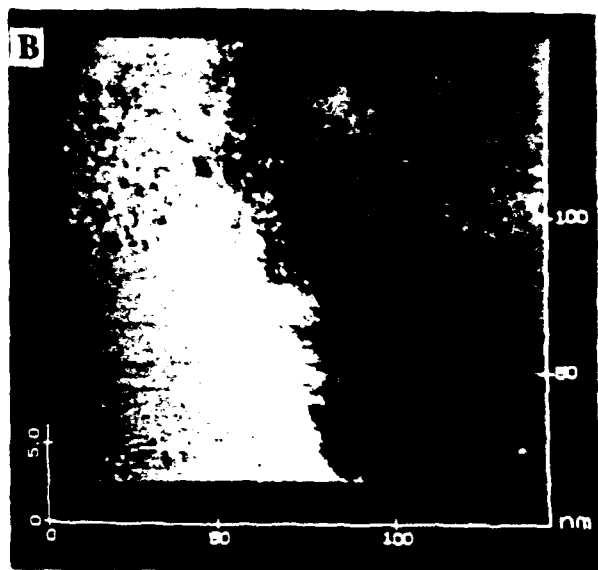
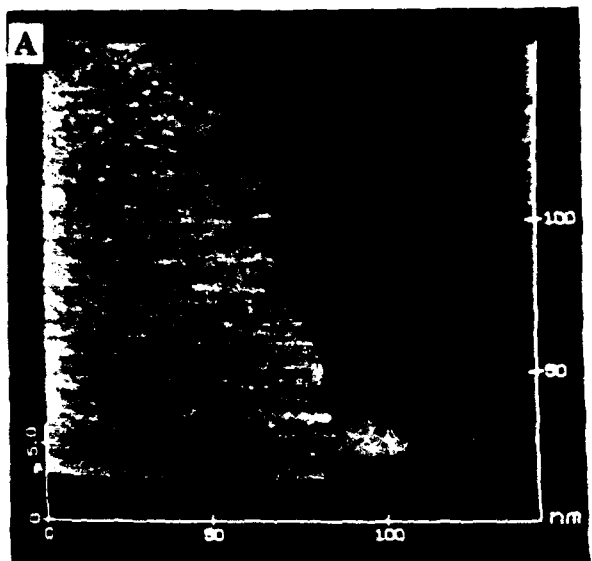


FIG 2

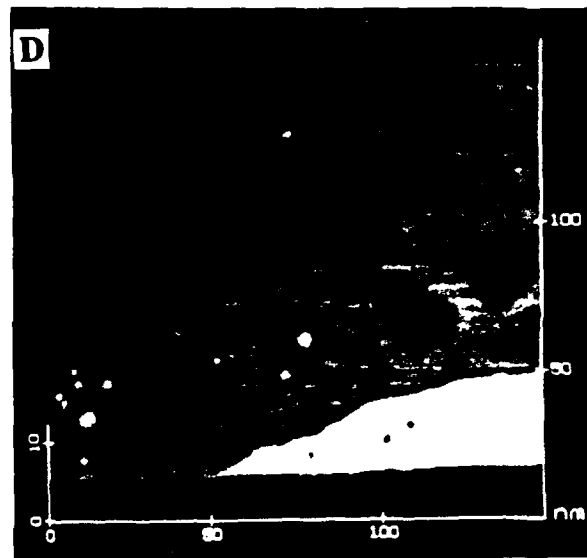
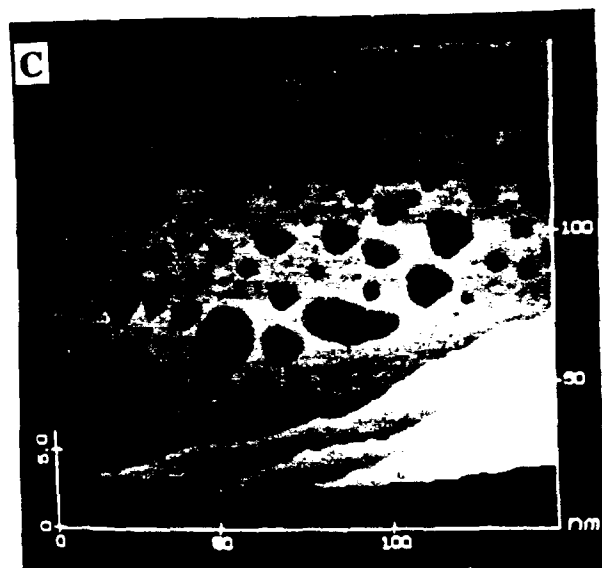
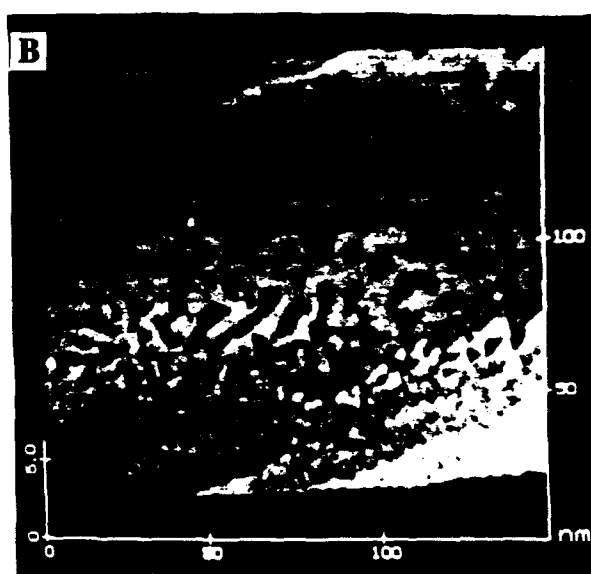
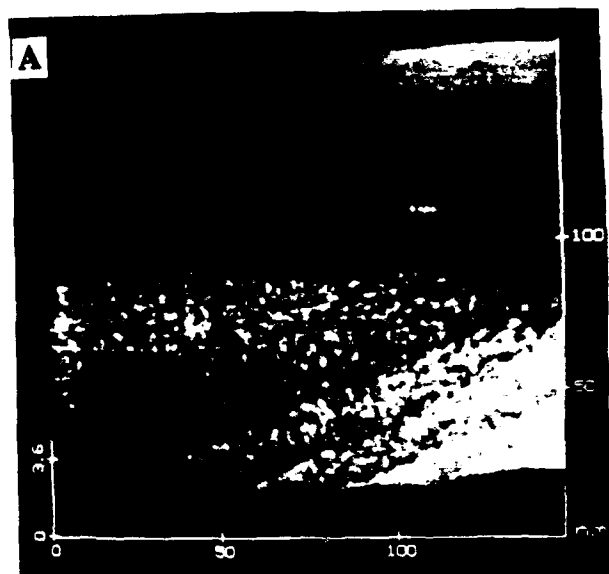


FIG 3